



Soft Matter

**Surface diffusion in glasses of rod-like molecules
posaconazole and itraconazole: Effect of interfacial
molecular alignment and bulk penetration**

Journal:	<i>Soft Matter</i>
Manuscript ID	SM-ART-02-2020-000353.R1
Article Type:	Paper
Date Submitted by the Author:	04-May-2020
Complete List of Authors:	Li, Yuhui; University of Wisconsin-Madison, School of Pharmacy Zhang, Wei; University of Wisconsin-Madison, School of Pharmacy; Genentech Inc Bishop, Camille; University of Wisconsin-Madison, Department of Chemistry Huang, Chengbin ; University of Wisconsin-Madison, School of Pharmacy Ediger, Mark; Univ of Wisconsin, Dept. of Chemistry Yu, Lian; University of Wisconsin Madison,

SCHOLARONE™
Manuscripts

1 **Surface diffusion in glasses of rod-like molecules posaconazole and itraconazole:**
2 **Effect of interfacial molecular alignment and bulk penetration**

3 Yuhui Li¹, Wei Zhang^{1,3}, Camille Bishop², Chengbin Huang¹, M. D. Ediger², Lian Yu^{1*}

4 ¹ School of Pharmacy, University of Wisconsin-Madison, Madison, WI, 53705, USA

5 ² Department of Chemistry, University of Wisconsin-Madison, Madison, WI, 53706, USA

6 ³ Current Address: Genentech Inc., South San Francisco, CA, 94080, USA

7

8

9 **Abstract.** The method of surface grating decay has been used to measure surface diffusion in the glasses
10 of two rod-like molecules posaconazole (POS) and itraconazole (ITZ). While structurally similar
11 antifungal medicines, ITZ forms liquid-crystalline phases while POS does not. Surface diffusion in these
12 systems is significantly slower than in the glasses of quasi-spherical molecules of similar volume when
13 compared at the glass transition temperature T_g . Between the two systems, ITZ has slower surface
14 diffusion. These results are explained on the basis of the near-vertical orientation of the rod-like
15 molecules at the surface and their deep penetration into the bulk where mobility is low. For molecular
16 glasses without extensive hydrogen bonds, we find that the surface diffusion coefficient at T_g decreases
17 smoothly with the penetration depth of surface molecules and the trend has the double-exponential form
18 for the surface mobility gradient observed in simulations. This supports the view that these molecular
19 glasses have a similar mobility vs depth profile and their different surface diffusion rates arise simply
20 from the different depths at which molecules are anchored. Our results also provide support for a
21 previously observed correlation between the rate of surface diffusion and the fragility of the bulk liquid.

22

23 **Keywords.** Glass, surface diffusion, posaconazole, itraconazole, rod-like molecule, liquid crystal,
24 mobility gradient.

25

26

27 Introduction

28 Surface mobility plays an important role in the physical stability of molecular glasses. Surface
29 molecules can diffuse much faster than bulk molecules,^{1,2,3} and this has been attributed to reduced local
30 caging effect and smaller elastic penalty for rearrangement.^{4,5} Surface mobility enables fast crystal
31 growth in molecular glasses, reducing the shelf life of amorphous drugs^{6,7} and motivating coating
32 technologies for stabilization.⁸ Surface mobility allows preparation of “ultra-stable glasses” by physical
33 vapor deposition, taking advantage of the fast equilibration of just-deposited molecules before they are
34 firmly embedded in the bulk.^{9,10}

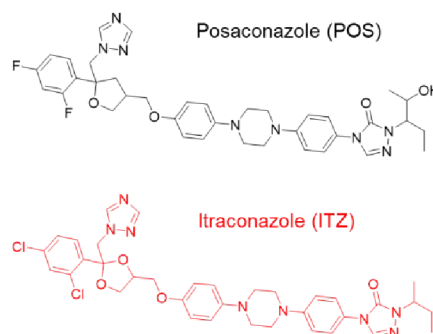
35
36 Surface diffusion can be measured by observing the evolution of surface contours driven by surface
37 tension.^{1,2,11,12,13,14} Previous work in this area has focused on molecular glasses containing quasi-
38 spherical molecules or slightly elongated molecules.³ Motivated

39 by recent attention to highly anisotropic glasses prepared with
40 non-spherical molecules,¹⁵ we have studied surface diffusion in
41 the glasses of two rod-like molecules, posaconazole (POS) and
42 itraconazole (ITZ) (see Scheme 1), both antifungal drugs.^{16,17}

43 While having similar structures, the two molecules differ in that
44 ITZ forms liquid crystals (LC),¹⁸ while POS does not.¹⁹ This
45 provides an opportunity to study the effect of bulk LC structure on
46 surface diffusion. We find that surface diffusion is significantly
47 slower in the glasses of POS and ITZ than in the glasses of quasi-
48 spherical molecules of similar volume. This is attributed to the near-vertical orientation of the rod-like
49 molecules at the surface and their deeper penetration into the bulk where mobility is low. Between the
50 two systems studied, ITZ has slower surface diffusion, likely a result of the deeper penetration of surface
51 molecules in this system.

52

53 Apart from investigating new types of molecules, this work was motivated by developing capabilities to
54 predict surface diffusion rates. Chen et al. have analyzed all published surface diffusion results on
55 molecular glasses and noted that the surface diffusion coefficient decreases smoothly with molecular
56 size for van der Waals systems (no extensive hydrogen bonds).³ They attributed this to a steep and
57 generic mobility gradient beneath the surface of a molecular glass. Larger molecules insert themselves



Scheme 1. Molecular structures of posaconazole (POS) and itraconazole (ITZ).

58 deeper into the bulk where mobility is lower, slowing down their center-of-mass diffusion. In this work
59 we extend their investigation to even deeper bulk penetration using the rod-like molecules and observe a
60 greater retardation of diffusion. Our results uphold the previous conclusion and our mobility vs depth
61 profile displays the double-exponential form characteristic of surface mobility gradient seen in
62 simulations.^{20,21} This finding is useful for predicting surface diffusion from molecular structures. We
63 also examine a previously observed correlation between the rate of surface diffusion and the fragility of
64 the bulk liquid.

65

66 **Experimental Section**

67 Posaconazole (POS, purity > 98%) was obtained from Biochempartner and itraconazole (ITZ, purity
68 > 99%) from Alfa Aesar. The materials were used as received. To make a surface grating, a master
69 pattern was placed on a viscous liquid of POS or ITZ at 363 K and was peeled off after vitrifying the
70 liquid at 298 K. This yielded a glass film with a sinusoidal surface contour. Master gratings of different
71 wavelengths were obtained as follows: for $\lambda = 1000$ nm and 1984 nm, plastic gratings purchased from
72 Rainbow Symphony were used; for $\lambda = 334$ nm, the masters were duplicated from a Blue-ray disc
73 through a UV-curing polymer (Norland Optical Adhesive 61); for $\lambda = 553$ nm, the masters were
74 duplicated from a glass grating (Spectrum Scientific) through the same polymer. All masters were
75 coated with 10 nm gold before use (Sputter deposition system, Leica ACE600). The thickness of each
76 embossed glass film was 50 – 100 μm , much larger than the wavelength of any surface grating used,
77 ensuring that the evolution of the top surface was unaffected by the substrate.

78

79 The flattening of a surface grating over time was monitored by Atomic Force Microscopy (AFM, Bruker
80 Veeco Multiple Mode IV) or laser diffraction. AFM was performed in the tapping mode at room
81 temperature; the height profile was Fourier transformed to obtain the amplitude of the sinusoidal surface.
82 Laser diffraction was measured in transmission and used to determine faster decay than feasible with
83 AFM. A HeNe laser ($\lambda = 632.8$ nm, Uniphase Corp.) passed through a sample film perpendicularly and
84 the first-order diffraction in transmission was recorded with a silicon amplified detector (Thorlabs)
85 interfacing with a National Instruments LabVIEW program. The grating amplitude was verified to be
86 proportional to the square root of diffraction intensity. The diffraction method was used only for POS

87 since the cloudiness of LC phases made transmission experiments difficult for ITZ. The two methods
 88 yielded identical results within experimental error when applied to the same decay process. During
 89 grating decay, the sample was purged with dry nitrogen and its temperature was controlled within 0.1 K
 90 with a Linkam microscope temperature stage or a custom-made mini-oven.

91

92 **Mullins' Theory of Surface Evolution**

93 According to Mullins,²² the amplitude h of a sinusoidal surface contour decreases exponentially over
 94 time, $h = h_0 \exp(-Kt)$, and the decay rate K is given by:

$$95 \quad K = Fq + Aq^2 + (A' + C)q^3 + Bq^4 \quad (1)$$

96 where

$$97 \quad q = 2\pi/\lambda$$

$$98 \quad F = \frac{\gamma}{2\eta}$$

$$99 \quad A = \frac{p_0\gamma\Omega^2}{(2\pi m)^{1/2}(kT)^{3/2}}$$

$$100 \quad A' = \frac{\rho_0 D_G \gamma \Omega^2}{kT}$$

$$101 \quad C = \frac{D_v \gamma \Omega}{kT}$$

$$102 \quad B = \frac{D_s \gamma \Omega^2 \nu}{kT}$$

103 In eq. (1), λ is the grating wavelength, γ is the surface tension, η the viscosity, p_0 the vapor pressure at
 104 equilibrated state, Ω the molecular volume, m the molecular weight, ρ_0 the vapor density at equilibrated
 105 state, D_G the diffusion coefficient of the vapor molecules in an inert atmosphere, D_v the self-diffusion
 106 coefficient in the bulk, ν the areal density of molecules on the surface, and D_s the surface diffusion
 107 coefficient. The different terms in eq. (1) correspond to different mechanisms of surface evolution:
 108 viscous flow (the F term), evaporation-condensation (A and A'), bulk diffusion (C), and surface

109 diffusion (B). For each decay mechanism, the decay
 110 rate has a characteristic dependence on the grating
 111 wavelength, useful for identifying the mechanism; for
 112 example, $K \propto \lambda^{-1}$ for viscous flow and $K \propto \lambda^{-4}$ for
 113 surface diffusion. Mullins' method has been applied to
 114 measure the surface diffusion of many materials, both
 115 crystalline²³ and amorphous.^{1,3} In the case of a glass-
 116 forming Lennard-Jones liquid, Malshe et al. showed by
 117 simulations that the surface diffusion constant
 118 determined by Mullins' method agrees with that
 119 calculated from the mean squared displacement of
 120 particles.²⁴

121

122 Results

123 Figure 1 shows the DSC traces of POS and ITZ. The
 124 two liquids have similar T_g s with the value for ITZ
 125 being slightly lower. The lower T_g of ITZ is consistent
 126 with the dielectric spectroscopy results,^{18,19} which show
 127 that ITZ has a shorter structural relaxation time at the
 128 same temperature. Different from POS, ITZ undergoes
 129 two phase transitions in the liquid state.¹⁸ Cooling from
 130 a high temperature, an isotropic liquid of ITZ
 131 transforms into a nematic phase ($T_{NI} = 363$ K) and then
 132 to a smectic phase ($T_{Sm/N} = 347$ K).

133

134 **Posaconazole (POS).** Figure 2 shows the typical decay
 135 kinetics of a POS surface grating recorded by laser
 136 diffraction (Figure 2a) and by AFM (Figure 2b). In
 137 each case, the decay was exponential, consistent with

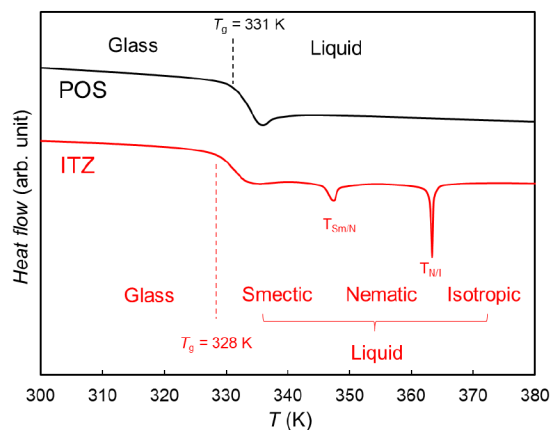


Figure 1. DSC traces of POS and ITZ during heating at 10 K/min. Both systems show a glass transition (T_g) and ITZ shows two LC

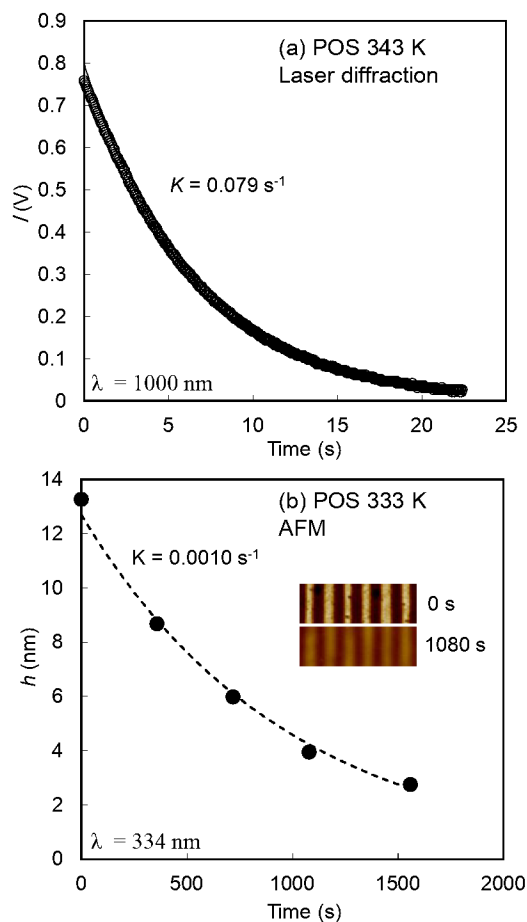


Figure 2. Typical decay kinetics of POS surface gratings. (a) At 343 K, recorded by laser diffraction ($\lambda = 1000$ nm). I is the diffraction intensity. (b) At 333 K recorded by AFM ($\lambda = 334$ nm). Inset: AFM images at two time points.

138 Mullins' theory.²² The data were fit to the function $\phi = \exp(-Kt)$, where ϕ is h/h_0 for AFM
 139 measurements and $(I/I_0)^{1/2}$ for diffraction measurements and K is the decay constant.

140

141 Figure 3a shows the decay constant K of POS at $\lambda = 334$ nm
 142 as a function of temperature. The structural
 143 relaxation time of the POS liquid¹⁸ is also shown for
 144 comparison; for this plot, we have extrapolated the
 145 experimental data below 331 K using the Vogel-Fulcher-
 146 Tammann (VFT) equation. At high temperatures, K
 147 closely tracks the structural relaxation time, $K \propto \tau_\alpha^{-1}$.
 148 Given that viscosity is generally proportional to τ_α , this
 149 indicates that viscous flow is the mechanism of surface
 150 flattening (the F term in eq. (1)). For this mechanism,
 151 the decay rate should be inversely proportional to the
 152 surface grating wavelength, $K \propto \lambda^{-1}$, and this was found
 153 to be the case (Figure 3b, see the 338 K result). This
 154 relation has been used to convert the K values measured
 155 at longer wavelengths to the values at $\lambda = 334$ nm so
 156 they can be included in Figure 3a to extend the
 157 measurement to higher temperatures.

158

159 Although viscous flow accounts for the decay rates
 160 observed at high temperatures, it does not at low
 161 temperatures (Figure 3a). The observed decay rate is
 162 "too fast" relative to viscous relaxation below 333 K (T_g
 163 + 2 K). This suggests a change of mechanism for surface evolution, as observed in other systems.¹
 164 Figure 3b shows that in this lower temperature region, K has a stronger dependence on the surface
 165 grating wavelength, $K \propto \lambda^{-4}$, which is expected for the surface diffusion mechanism. Thus, we assign the
 166 mechanism of surface evolution to surface diffusion at low temperatures and use the observed decay

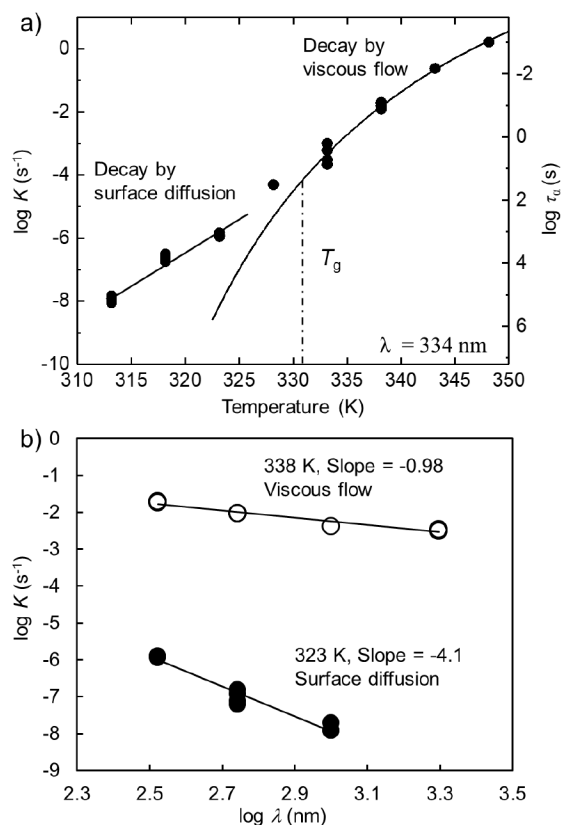


Figure 3. (a) Decay constant K of a POS surface grating at $\lambda = 334$ nm as a function of temperature. At high temperatures, K tracks the structural relaxation time τ_α (second y axis) indicating viscous flow controls surface evolution. Decay becomes faster below $T_g + 2$ K, indicating a change of surface flattening mechanism. (b) Wavelength dependence of K at two temperatures indicating decay by viscous flow at high temperatures and by surface diffusion at low temperatures.

167 rates to calculate the surface diffusion coefficients D_s (Figure 4). For this calculation, we assume $\gamma =$
 168 0.05 N/m, a typical value for organic liquids, and obtain $\Omega = 0.92 \text{ nm}^3$ (molecular volume) from the
 169 density of a POS glass (1.27 g/cm³, assumed to be the same as that an ITZ glass²⁵) and its molecular
 170 weight (700.8 g/mol). For this rod-like molecule, we estimate its areal density at the liquid/vapor
 171 interface by taking into account its preferred orientation. Bishop et al. used NEXAFS to show that POS
 172 molecules are nearly vertical at the liquid/vapor interface.²⁶ Thus we estimate the areal density using:
 173 $\nu \approx L/\Omega = 2.8 \text{ nm}^{-2}$, where L is the length of a POS molecule (2.6 nm, taken from its crystal structure).²⁷
 174 If POS is treated as a spherical molecule at the surface as opposed to an oriented rod, we obtain $\nu \approx$
 175 $\Omega^{-2/3} = 1.0 \text{ nm}^{-2}$ and the calculated D_s would be larger by a factor of 3; given the 5 order of magnitude
 176 spread of surface diffusion coefficients (Figure 4), this is
 177 a relatively small effect.

178 Figure 4 compares the surface diffusion coefficient D_s of
 179 POS and other molecular glasses: *ortho*-terphenyl
 180 (OTP),²⁸ *tris*-naphthyl benzene (TNB),²⁹ griseofulvin
 181 (GSF),³⁰ indomethacin (IMC),¹ and polystyrene (PS)
 182 oligomers (1110 and 1700 g/mole).³¹ Figure 4 also
 183 shows the bulk diffusion coefficients D_v of the same
 184 systems when available.^{32,33,34,35} After scaling the
 185 temperature by T_g , the D_v values cluster to a “master
 186 curve”. Relative to this, the D_s values are all larger and
 187 do not collapse into a single curve. Note that of all the
 188 systems studied to date, POS has the slowest surface
 189 diffusion in this comparison: its D_s at T_g , $\sim 10^{-17} \text{ m}^2/\text{s}$ (estimated by extrapolation), is 5 orders of
 190 magnitude smaller than the value for OTP. In addition, the D_s of POS has the strongest temperature
 191 dependence, with an activation energy (389 kJ/mol) close to that for bulk diffusion. The slow surface
 192 diffusion of POS will be discussed later and attributed to the near-vertical orientation of the surface
 193 molecules and their deep penetration into the bulk.

194

195

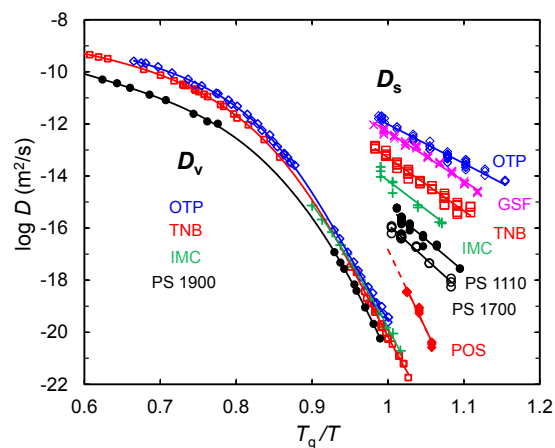


Figure 4. Surface diffusivity in POS and other molecular glasses. T_g is the onset temperature measured by DSC during heating at 10 K/min after cooling at the same rate.

196 **Itraconazole (ITZ).** Figure 5a shows the surface-
 197 grating decay constant K of ITZ at $\lambda = 334$ nm as a
 198 function of temperature. The bulk structural relaxation
 199 time¹⁸ is also shown for comparison. As in the case of
 200 POS, the relation $K \propto \tau_\alpha^{-1}$ is observed at high
 201 temperatures, indicating surface evolution by viscous
 202 flow. This is confirmed by wavelength tests (Figure 5b).
 203 At both 323 K and 333 K, we observe the relation $K \propto$
 204 λ^{-1} , as expected for the viscous-flow mechanism.

205
 206 The key difference between ITZ and POS is that in ITZ,
 207 viscous flow controls surface evolution down to a
 208 lower temperature relative to T_g . In ITZ, K tracks τ_α
 209 down to $T_g - 5$ K (Figure 5a), whereas in POS, this is
 210 the case only down to $T_g + 2$ K (Figure 3a), below
 211 which surface diffusion is fast enough to be the decay
 212 mechanism (Figure 3b). Thus, surface diffusion in ITZ
 213 must be slower than that in POS at the same
 214 temperature relative to T_g .

215
 216 To see the point above more clearly, in Figure 6, we
 217 plot the decay constant K against the bulk relaxation
 218 time τ_α for both systems. This allows a comparison of
 219 the two surface processes at the same bulk mobility. At
 220 high temperatures (short τ_α), we find $K \propto \tau_\alpha^{-1}$,
 221 confirming surface evolution by viscous flow. In this
 222 region, the two systems have very similar decay rates
 223 at a common τ_α (bulk mobility), as expected for this
 224 mechanism. At low temperatures (long τ_α), the

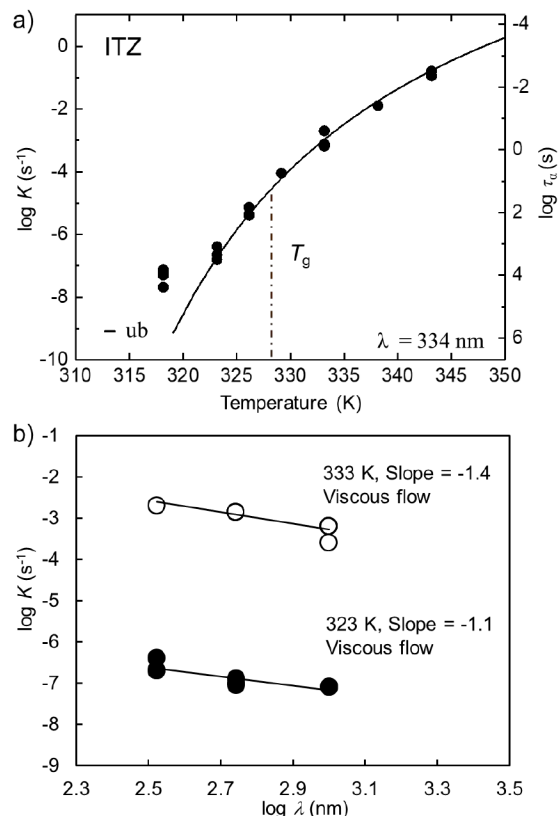


Figure 5. (a) Surface grating decay rate K of ITZ at $\lambda = 334$ nm as a function of temperature. “ub” indicates an upper bound from no significant decay in 250 days. (b) K as a function of grating wavelength λ at 323 K and

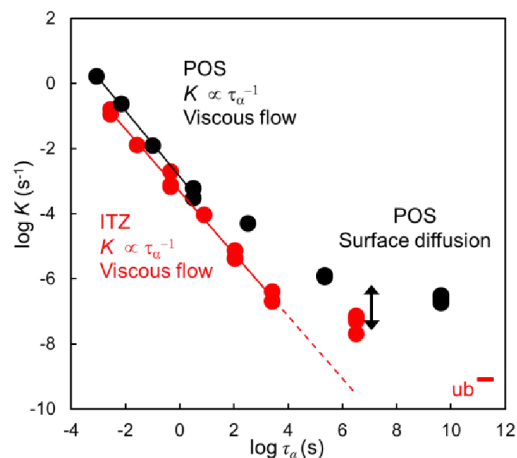


Figure 6. Surface-grating decay constant K at $\lambda = 334$ nm plotted against the bulk relaxation time τ_α for ITZ and POS. At high temperatures (short τ_α), $K \propto \tau_\alpha^{-1}$ holds, indicating surface evolution by viscous flow. At low temperatures (long τ_α), faster decay is observed signaling a new decay mechanism.

225 observed decay is faster relative to viscous flow, suggesting a change of decay mechanism. For POS, the
 226 new decay mechanism was shown to be surface diffusion by a wavelength test (Figure 3b). It is likely
 227 that the ITZ undergoes the same transition to surface diffusion at the lowest temperature studied (we
 228 have not verified this by wavelength test due to the very slow decay rates). Under this assumption, we
 229 can assess the relative rates of surface diffusion in the two systems: in POS, the transition from viscous
 230 flow to surface diffusion occurs at a much higher bulk mobility ($\tau_\alpha \approx 3$ s) than in ITZ ($\tau_\alpha \approx 3000$ s). Thus,
 231 surface diffusion in POS is fast enough to be the decay mechanism when bulk mobility is relatively high,
 232 but this does not happen in ITZ even at a much lower bulk mobility. From Figure 6, we estimate surface
 233 diffusion in ITZ to be ~ 20 times slower than that of POS at $\tau_\alpha \approx 10^7$ s (double-sided arrow).
 234

235 Discussion

236 The main result of this work is that surface diffusion is significantly slower in the glasses of the rod-like
 237 molecules POS and ITZ than in the previously studied systems (Figure 4). Between POS and ITZ,
 238 surface diffusion is slower in ITZ (Figure 6). We now discuss these results and suggest that the slow
 239 surface diffusion is a consequence of the deep penetration of the nearly vertically orientated surface
 240 molecules. We also use the new results to test a previously reported relation between surface mobility
 241 and bulk liquid fragility.
 242

243 In Figure 7, we illustrate the essential difference
 244 between the surface structures of liquids composed
 245 of quasi-spherical molecules and rod-like molecules
 246 (POS and ITZ). For a liquid of quasi-spherical
 247 molecules, each surface molecule penetrates into the
 248 bulk by approximately its diameter $d \approx \Omega^{1/3}$, where
 249 Ω is the molecular volume. In the case of POS,
 250 Bishop et al. have shown by NEXAFS that the rod-
 251 like molecules tend to be vertically aligned with $\theta_z \approx$
 252 33° , where θ_z is the average angle between the long
 253 axis of the molecule \mathbf{n}_L and the surface normal \mathbf{n}_z .²⁶

254 (For this discussion, we take each rod-like molecule as centrosymmetric and θ_z to be positive.) Preferred

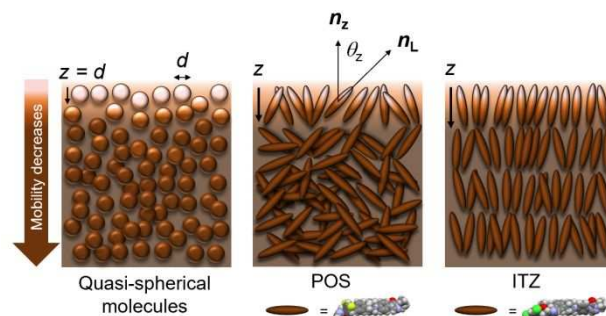


Figure 7. Different surface molecular structures of liquids of quasi-spherical molecules and rod-like molecules POS and ITZ. While both rod-shaped, ITZ molecules form a smectic LC phase whereas POS molecules produce an isotropic liquid. For quasi-spherical molecules, the depth of penetration of a surface molecule is approximately its diameter, $z = d$. The depth of penetration can be significantly larger for vertically oriented rod-like molecules. This anchors them deeper in the bulk where mobility is low, hindering their center-of-mass diffusion.

orientation at interfaces has been observed for many non-spherical molecules and is a result of free-energy minimization in an environment lacking translational symmetry.^{36, 37, 38} We estimate the depth of penetration for a surface molecule as $z = L \cos \theta_z$, where $L \approx 2.6$ nm is the length of a POS molecule in its crystals.²⁷ This yields a penetration depth of 2.2 nm, more than twice the value for a spherical molecule of the same volume ($d = 0.97$ nm), a direct result of preferred orientation.

260

In the case of ITZ, the bulk liquid is a smectic LC in the temperature range of our study, and this can influence the orientational order of surface molecules. In the bulk smectic phase, rod-like ITZ molecules tend to be parallel with the LC director forming an average angle of 27° .¹⁸ At the vapor interface, the LC director favors a vertical orientation (homeotropic alignment); this is seen from the annealing behavior of a vapor-deposited glass film.³⁹ The surface anchoring effect has been observed with other rod-like, LC-forming molecules.⁴⁰ Furthermore, simulations have shown that surface molecules of a LC can be slightly more vertically aligned than in the bulk.⁴¹ Together, these results indicate that ITZ molecules favor a vertical orientation at the free surface and that their orientational order should be higher than that of POS molecules. From its bulk orientational order and its length of 2.8 nm (in crystals),⁴² we estimate the depth of penetration for an ITZ surface molecule to be 2.5 nm.

282

Our central hypothesis is that the diffusion rate of surface molecules is determined by their depth of penetration into the bulk. Because mobility

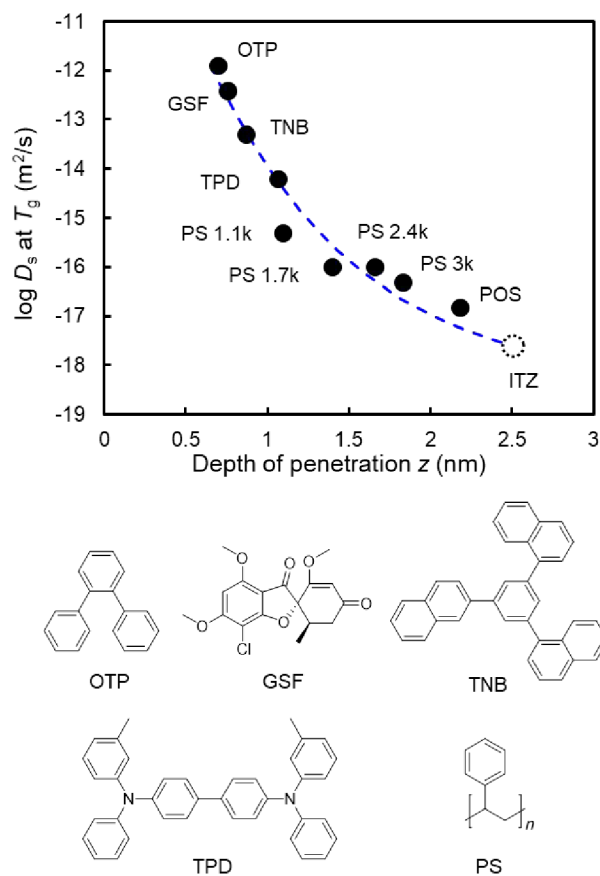


Figure 8. Surface diffusion coefficient D_s at T_g as a function of the penetration depth z . For quasi-spherical molecules OTP, GSF, and TNB, $z \approx d$ (mean molecular size). For rod-like molecules TPD, POS, and ITZ, $z = L \cos \theta_z$, where L is the length of the molecule and θ_z is the average angle between the molecular long axis and the surface normal. For chain-like PS oligomers, $z = R_{ee} \cos \theta_{zee}$, where R_{ee} is the end-to-end distance and θ_{zee} the average angle between the R_{ee} vector and the surface normal. The curve is a fit of the experimental data using a double-exponential form (eq. (2)) thought to represent the surface mobility gradient of a molecular glass. The arrow indicates the estimated D_s for ITZ based on extrapolation of the fitting curve.

286 decreases rapidly across a vapor/glass interface, we expect the translational mobility of a surface
 287 molecule to be limited by its bottom part where mobility is the lowest, even if its top part is in a region
 288 of higher mobility. We test this idea in Figure 8 by plotting the surface diffusion coefficient at T_g as a
 289 function of the penetration depth of surface molecules, using data from this work and the literature. The
 290 molecular structures of the systems included are shown at the bottom of Figure 8 and in Scheme 1;
 291 Table 1 contains the numerical values. In this analysis, we regard OTP, GSF, and TNB as quasi-
 292 spherical molecules and use the mean molecular size $d = \Omega^{1/3}$ to represent the depth of penetration. For
 293 the mildly elongated TPD, penetration depth is estimated in the same way as POS and ITZ: $z = L \cos \theta_z$,
 294 where $L \approx 1.7$ nm and $\theta_z \approx 51^\circ$ is obtained by atomistic MD simulations.⁴⁸ This yields $z = 1.1$ nm,
 295 slightly larger than the mean molecular size ($d = 0.9$ nm). For chain-like PS oligomers, penetration depth
 296 is calculated from $z = R_{ee} \cos \theta_z$, where R_{ee} is the end-to-end distance⁴³ and θ_z the average angle between
 297 the R_{ee} vector and the surface normal.⁵⁰ Given that hydrogen bonds have an independent effect on
 298 surface diffusion from molecular dimensions,³ Figure 8 only includes systems without extensive
 299 hydrogen bonds. Though hydrogen bonds might be present in a POS liquid, their contribution to the total
 300 vaporization energy is negligible ($\sim 5\%$, based on a group-additivity calculation^{3,44}) and we include this
 301 system in the analysis.

302

303

Table 1. Surface diffusion coefficients D_s of molecular glasses and other properties.

	T_g (K)	M (g/mol)	ρ (g/cm ³)	d (nm)	L or R_{ee} (nm)	S_z	θ_z (deg.)	z (nm)	$\log D_s$ at T_g (m ² /s)
OTP	246	230.3	1.12 ⁴⁵	0.70	—	—	—	0.70 ^a	-11.9 ²⁸
GSF	361	352.8	1.35 ⁴⁶	0.76	—	—	—	0.76 ^a	-12.4 ³⁰
TNB	347	456.6	1.15 ⁴⁷	0.87	—	—	—	0.87 ^a	-13.3 ²⁹
TPD	330	516.7	1.19 ²	0.90	1.7 ⁴⁸	0.1 ⁴⁸	51	1.1	-14.2 ²
PS1100	307	990	1.03 ⁴⁹	1.17	2.1 ⁴³	-0.1 ⁵⁰	58	1.1	-15.3 ³¹
PS1700	319	1600	1.03 ⁴⁹	1.37	2.6 ⁴³	-0.1 ⁵⁰	58	1.4	-16.0 ³¹
PS2400	337	2264	1.03 ⁴⁹	1.54	3.1 ⁴³	-0.1 ⁵⁰	58	1.7	-16.0 ¹³
PS3000	343	2752	1.03 ⁴⁹	1.64	3.5 ⁴³	-0.1 ⁵⁰	58	1.8	-16.3 ¹¹
POS	331	700.8	1.27 ^b	0.97	2.6 ²⁷	—	33 ²⁶	2.2	-16.8
ITZ	328	705.6	1.27 ²⁵	0.97	2.8 ⁴²	0.7 ^c	27 ¹⁸	2.5	(-17.8) ^d

304

^a The penetration depth of these quasi-spherical molecules are assumed to be the same as their mean molecular size, $z = d$.

305

^b Assumed to be the same as that of ITZ.

306

^c Calculated from the S_z value from Ref. 18 (bulk value).

307

^d Estimated based on trends in Figures 8 and 9.

308

309 Based on our hypothesis, we expect the rate of surface diffusion to decrease with the depth of
 310 penetration. This is indeed observed in Figure 8. We see a smooth falling trend starting from the three
 311 quasi-spherical molecules (OTP, GSF, and TNB), to the mildly elongated TPD, to the chain-like PS
 312 oligomers, and finally to the rod-like POS. These systems cover a 5 orders of magnitude in D_s and a
 313 penetration depth from 0.7 nm (OTP) to 2.2 nm (POS). The open circle indicates the estimated D_s for
 314 ITZ by extrapolation (see below).

315

316 The smooth trend observed in Figure 8 suggests that the molecular glasses considered have a similar
 317 mobility vs depth profile when compared at T_g and that the different surface diffusion rates simply
 318 reflect the different depths at which surface molecules are anchored. In principle, each system in Figure
 319 8 has its own mobility vs depth profile. But given the smooth trend observed, a reasonable first
 320 approximation is to treat it as a generic mobility profile for van der Waals molecular glasses at T_g . One
 321 support for this notion is that the profile in Figure 8 is consistent with the “double-exponential” form for
 322 surface mobility gradient observed in simulations:^{20,21}

$$323 \quad \tau(z) = \tau_\alpha \exp[-A \exp(-z/\xi)] \quad (2)$$

324 where τ_α is the bulk relaxation time, A is a “surface-enhancement” factor, and ξ is the dynamical
 325 correlation length. This form is thought to arise from an activation barrier for local relaxation that
 326 increases exponentially with depth. Phan and Schweitzer have rationalized this as a consequence of
 327 geometric-like, layer-wise transfer of caging constraint from the surface to the bulk.^{51,52} The curve in
 328 Figure 8 is a fit of the data to eq. (2). In this fitting, we assume $\tau_\alpha = 10$ s at T_g and estimate $\tau(z)$ from the
 329 equation: $D_s(z) = d^2/[4\tau(z)]$. In essence, the last equation assumes the observed D_s is determined by the
 330 local mobility at the depth of penetration z . Figure 8 shows that eq. (2) can accurately describe the
 331 experimental data. This argues that despite their different chemistry, the molecular glasses considered
 332 have a similar mobility profile $\tau(z)$ at T_g . From this fitting, we obtain $\xi = 1$ nm, consistent with the
 333 values obtained from simulations.^{20,21}

334

335 We now turn to the slower surface diffusion of ITZ relative to POS. Based on the ideas developed above,
 336 the simplest explanation is that the deeper penetration of ITZ surface molecules (2.5 nm vs 2.2 nm)
 337 anchor them deeper in the bulk where mobility is lower. This leads to slower center-of-mass diffusion.

338 In Figure 8, we extrapolate the double-exponential fit of the experimental data points to the penetration
 339 depth of ITZ to estimate its surface diffusion rate. This yields $\log D_s$ (m^2/s) = -17.6 at T_g , in agreement
 340 with our finding that surface diffusion is slower in ITZ than in POS (Figure 6).

341

342 Chen et al. have performed a similar analysis to that presented in Figure 8 using the mean molecular size
 343 d to represent the penetration depth.³ Their D_s vs d plot includes all the systems in Figure 8 except for
 344 POS and ITZ. Their plot shows a smooth decreasing trend, but when included in their plot, the rod-like
 345 molecules are outliers. For example, the D_s of POS is 30 times smaller than that of PS1110, but the two
 346 molecules have similar d values (Table 1). This is because d can represent the penetration depth of
 347 quasi-spherical molecules but not rod-shaped molecules like POS. Because of its near vertical
 348 orientation, POS penetrates deeper into the bulk than a spherical molecule of the same volume. It is
 349 interesting to note that for the chain-like PS
 350 oligomers, d is not greatly different from the
 351 estimated depth of penetration z (Table 1). This is
 352 because the R_{ce} vector of PS tends toward a parallel
 353 orientation at the surface,⁵⁰ reducing the depth of
 354 penetration.

355

356 Correlation between Surface Diffusion and Bulk

357 **Fragility.** Chen et al.⁵³ reported a correlation between

358 the rate of surface diffusion and the fragility of the
 359 bulk liquid, with stronger liquids having slower
 360 surface diffusion when compared at T_g . This
 361 correlation is useful for predicting surface mobility
 362 from the dynamics of bulk liquids. In Figure 9, we
 363 test this correlation using the data from this work and
 364 the recently reported data on GSF.³⁰ We plot the D_s
 365 value at T_g against the viscosity of the bulk liquid at
 366 $1.25 T_g$ (Figure 9a), used as a measure of fragility.⁵³
 367 While the m index (slope of each curve in Figure 9a
 368 taken at T_g) is often used to measure fragility, it is

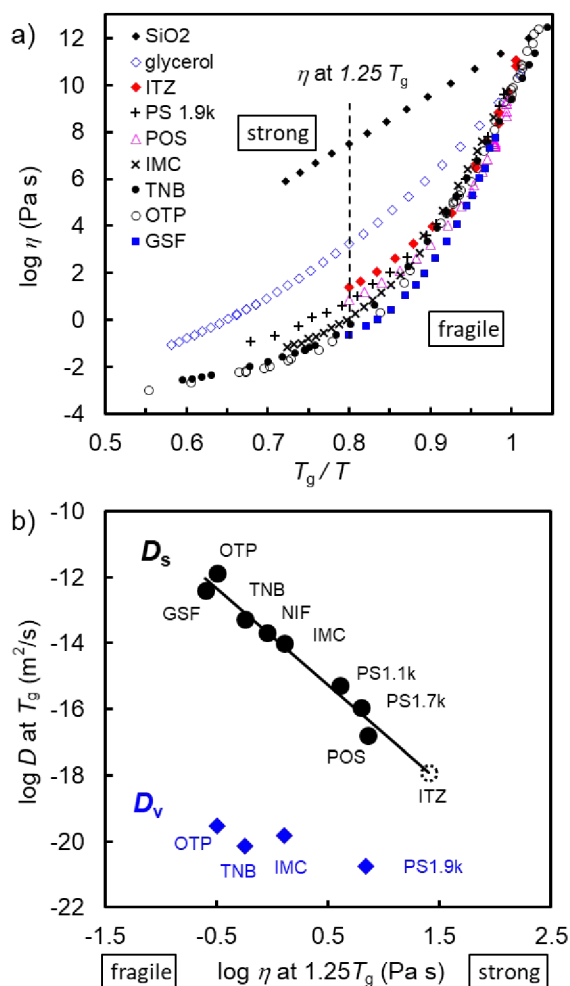


Figure 9. (a) Angell plot of viscosity of glass-forming liquids as a function of temperature scaled by DSC T_g . Viscosity at $1.25 T_g$ is used as a measure of fragility. (b) Correlation between diffusion coefficients and bulk liquid fragility. The ITZ point (open circle) is estimated by extrapolating the trend for the other data points to the viscosity of ITZ at $1.25 T_g$.

369 sensitive to errors of slope-taking in a temperature region where viscosity varies rapidly.⁵⁴ Our choice
370 has the advantage of comparing experimental viscosity at a temperature at which displacement from the
371 Arrhenius behavior is large. For GSF, the viscosity data are from Ref. 55, with a small extrapolation to
372 high temperature through a VFT fit (Figure S1). For POS and ITZ, the literature viscosity is extrapolated
373 with the aid of τ_α assuming the two have the same temperature dependence (Figures S2 and Figure
374 S3).¹⁹ Figure 9b shows that the new data points for GSF and POS both fall on the trend of the previous
375 data, confirming the conclusion that stronger liquids have slower surface diffusion. In contrast to the
376 strong dependence of D_s on fragility, the bulk diffusion coefficient D_v has a much weaker dependence (if
377 at all). The surface diffusion coefficient of ITZ can be estimated by extrapolating the trend to the
378 viscosity of ITZ at $1.25 T_g$. This yields $\log D_s$ (m²/s) = -17.9, in good agreement with the estimate in
379 Figure 8, $\log D_s$ (m²/s) = -17.6, using the penetration depth of ITZ molecules. The average of these two
380 values is entered in Table 1 as a preliminary result for ITZ.

381

382 According to Chen et al.,⁵³ the correlation in Figure 9 is interpreted as follows. Fragility measures how
383 easily a liquid's dynamics is excited when temperature is raised above T_g ; strong liquids resist this
384 excitation, while fragile liquids is excited easily. The change of molecular environment from the bulk to
385 the surface can also be regarded as a form of excitation (loss of nearest neighbors and decrease of
386 density) and a stronger liquid might be expected to resist this excitation more than a fragile liquid. In its
387 application to polymer melts, the elastically collective nonlinear Langevin equation (ECNLE) theory
388 makes a connection between fragility and the relative importance of cage constraint and elastic penalty
389 in segmental rearrangement and associates high fragility with dominance by elastic penalty.⁵⁶
390 Application of the theory to surface dynamics^{51,52} could provide a quantitative understanding of the
391 observed correlation in Figure 9.

392

393 **Conclusion**

394 In summary, the method of surface grating decay has been used to measure surface diffusion in the
395 glasses of two rod-like molecules POS and ITZ. Despite their similarity, the two systems differ in that
396 ITZ forms liquid-crystalline phases while POS does not. We find that surface diffusion in these systems
397 is significantly slower than in the glasses of quasi-spherical molecules of similar volume when
398 compared at T_g . This is attributed to the near-vertical orientation of the rod-like molecules at the surface,

399 allowing deep penetration into the bulk where mobility is low. At the same bulk mobility, ITZ has
400 slower surface diffusion than POS. This is attributed to a deeper penetration of the ITZ surface
401 molecules into the bulk.

402

403 We find that for van der Waals molecular glasses (without extensive hydrogen bonds), the surface
404 diffusion rate slows down smoothly with the depth of penetration of surface molecules (Figure 8). The
405 mobility vs depth profile is in good agreement with the double-exponential form observed by
406 simulations and explained by the ECNLE theory. This argues for a generic surface mobility gradient for
407 molecular glasses and the different surface diffusion rates simply reflect the different depths at which
408 surface molecules are anchored. This picture, if valid, allows the use of surface diffusion rate as a probe
409 for the surface mobility gradient, a topic of considerable current interest²⁰ and a challenging target for
410 direct experimental investigations.

411

412 The smooth trend of surface diffusivity as a function of the penetration depth of surface molecules is
413 potentially useful for predicting surface mobility (Figure 8). For quasi-spherical molecules, the
414 penetration depth is simply the molecular size. For chain-like and rod-like molecules, the penetration
415 depth depends on the orientation of surface molecules relative to the interface and this can be
416 determined by experimental techniques such as NEXAFS²⁶ and SFG⁵⁷ and by MD simulations.⁴⁸ For the
417 purpose of predicting surface mobility, another intriguing prospect is to use the correlation between the
418 rate of surface diffusion and the fragility of the bulk liquid (Figure 9).

419

420 The surface mobility trend allows contact with recent studies of physical vapor deposition. During vapor
421 deposition, surface mobility allows equilibration leading to formation of high stability, high density
422 glasses.⁹ While the measure of surface mobility most relevant for vapor deposition may not be surface
423 diffusion,³ Figure 8 allows the speculative conclusion that the best possible glass packing (the “ideal
424 glass”) would be most easily approached with small molecules. Indeed, recent experiments have shown
425 that ethylbenzene and toluene can closely approach ideal glass packing when prepared by vapor
426 deposition.^{58,59,60}

427

428 To our knowledge, this work is the first to study the surface diffusion of an anisotropic organic solid (the
429 vitrified liquid crystal of ITZ). We find that surface diffusion in ITZ is slower than that in the similar but

430 non-LC system POS. At present it is unclear whether the effect is purely a result of the deeper
431 penetration of ITZ molecules or reflects further constraints by the bulk crystalline phase. Further work in
432 this area will provide insight on surface mobility in crystalline solids.

433

434 **Supporting Information**

435 Viscosity and structural relaxation time for GSF, POS and ITZ.

436

437 **Conflicts of interest**

438 There are no conflicts of interest to declare.

439

440 **Acknowledgements**

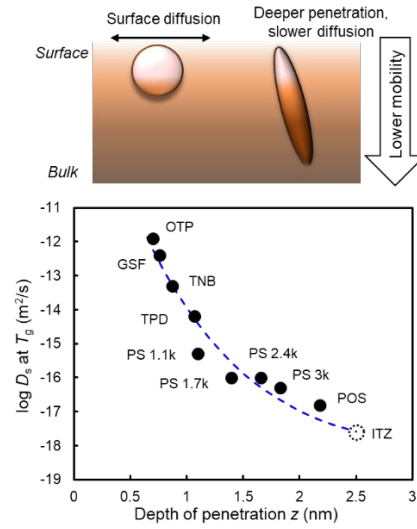
441 This research was primarily supported by NSF through the University of Wisconsin Materials Research
442 Science and Engineering Center (Grant DMR-1720415). We thank Paul Voyles for helpful discussions.

443

444 **References**

-
- ¹ L. Zhu, C. W. Brian, S. F. Swallen, P. T. Straus, M. D. Ediger and L. Yu, *Phys. Rev. Lett.*, 2011, **106**, 256103.
 - ² Y. Zhang, R. Potter, W. Zhang and Z. Fakhraai, *Soft Matter*, 2016, **12**, 9115-9120.
 - ³ Y. S. Chen, Z. X. Chen, M. Tylinski, M. D. Ediger and L. Yu, *J. Chem. Phys.*, 2019, **150**, 024502.
 - ⁴ J. D. Stevenson and P. G. Wolynes, *J. Chem. Phys.*, 2008, **129**, 234514.
 - ⁵ S. Mirigian and K. S. Schweizer, *J. Chem. Phys.*, 2015, **143**, 244705.
 - ⁶ Y. Sun, L. Zhu, K. L. Kearns, M.D. Ediger and L. Yu, *Proc. Natl. Acad. Sci.*, 2011, **108**, 5990.
 - ⁷ T. Wu and L. Yu, *Pharm. Res.*, 2006, **23**, 2350.
 - ⁸ Y. Li, J. Yu, S. Hu, Z. Chen, M. Sacchetti, C.C. Sun and L. Yu, *Mol. Pharm.*, 2019, **16**, 1305.
 - ⁹ S. F. Swallen, K. L. Kearns, M. K. Mapes, Y. S. Kim, R. J. McMahon, M. D. Ediger, T. Wu, L. Yu and S. Satija, *Science*, 2007, **315**, 353.
 - ¹⁰ L. Berthier, P. Charbonneau, E. Flenner and F. Zamponi, *Phys. Rev. Lett.*, 2017, **119**, 188002.
 - ¹¹ Y. Chai, T. Salez, J. D. McGraw, M. Benzaquen, K. Dalnoki-Veress, E. Raphaël and J. A. Forrest, *Science*, 2014, **343**, 994-999.
 - ¹² Z. Fakhraai and J. A. Forrest, *Science*, 2008, **319**, 600-604.
 - ¹³ Z. Yang, Y. Fujii, F. K. Lee, C. H. Lam and O. K. Tsui, *Science*, 2010, **328**, 1676-1679.
 - ¹⁴ P. E. Acosta-Alba, O. Kononchuk, C. Gourdel and A. Claverie, *J. Appl. Phys.*, 2014, **115**, 134903.
 - ¹⁵ M. D. Ediger, J. J. de Pablo and L. Yu, *Acc. Chem. Res.*, 2019, **52**, 407.
 - ¹⁶ E. J. Rachwalski, J. T. Wierzchowicz and M. H. Scheetz, *Ann. Pharm.*, 2008, **42**, 1429.
 - ¹⁷ M. Boogaerts, D. J. Winston, E. J. Bow, G. Garber, A. C. Reboli, A. P. Schwarzer, N. Novitzky, A. Boehme, E. Chwetzoff and K. De Beule, *Annals of internal medicine*, 2001, **135**, 412.
 - ¹⁸ M. Tarnacka, K. Adrjanowicz, E. Kaminska, K. Kaminski, K. Grzbowska, K. Kolodziejczyk, P. Włodarczyk, L. Hawelek, G. Garbacz, A. Kocot and M. Paluch, *Phys. Chem. Chem. Phys.*, 2013, **15**, 20742.

-
- ¹⁹ K. Adrjanowicz, K. Kaminski, P. Wlodarczyk, K. Grzybowska, M. Tarnacka, D. Zakowiecki, G. Garbacz, M. Paluch and S. Jurga, *Mole. Pharm.*, 2013, **10**, 3934.
- ²⁰ P. Scheidler, W. Kob and K. Binder, *Europhys. Lett.*, 2002, **59**, 701
- ²¹ K. S. Schweizer and D. S. Simmons, *J. Chem. Phys.*, 2019, **151**, 240901.
- ²² W.W. Mullins, *J. Appl. Phys.*, 1959, **30**, 77.
- ²³ P. S. Maiya and J. M. Blakely, *J. Appl. Phys.*, 1967, **38**, 698-704.
- ²⁴ R. Malshe, M. D. Ediger, L. Yu and J. J. de Pablo, *J. Chem. Phys.*, 2011, **134**, 194704.
- ²⁵ K. Six, G. Verreck, J. Peeters, M. Brewster and G. V. D. Mooter, *J. Pharm.Sci.*, 2004, **93**, 124
- ²⁶ C. Bishop, J. L. Thelen, E. Gann, M. F. Toney, L. Yu, D. M. DeLongchamp and M. D. Ediger, *Proc. Natl. Acad. Sci.*, 2019, **116**, 21421.
- ²⁷ D. K. McQuiston, M. R. Mucalo and G. C. Saunders, *J. Mol. Struc.*, 2019, **1179**, 477.
- ²⁸ W. Zhang, C. W. Brian and L. Yu, *J. Phys. Chem. B.*, 2015, **119**, 5071.
- ²⁹ S. Ruan, W. Zhang, Y. Sun, M. D. Ediger and L. Yu, *J. Chem. Phys.* 2016, **145**, 064503.
- ³⁰ C. Huang, S. Ruan, T. Cai and L. Yu, *J. Phys. Chem. B.*, 2017, **121**, 9463.
- ³¹ W. Zhang and L. Yu, *Macromolecules.*, 2016, **49**, 731.
- ³² M. K. Mapes, S. F. Swallen and M. D. Ediger, *J. Phys. Chem. B.*, 2006, **110**, 507.
- ³³ S. F. Swallen, K. Traynor, R. J. McMahon, M. D. Ediger and T. E. Mates, *J. Phys. Chem. B.*, 2009, **113**, 4600.
- ³⁴ S. F. Swallen, and M. D. Ediger, *Soft Matter*, 2011, **7**, 10339.
- ³⁵ O. Urakawa, S. F. Swallen, M. D. Ediger and E. D. von Meerwall, *Macromolecules*, 2004, **37**, 1558.
- ³⁶ H. Kimura and H. Nakano, *J. Phys. Soc. Japan*, 1985, **54**, 1730.
- ³⁷ A. Haji-Akbari and P. G. Debenedetti, *J. Chem. Phys.*, 2015, **143**, 214501
- ³⁸ M. Sadati, H. Ramezani-Dakhel, W. Bu, E. Sevgen, Z. Liang, C. Erol, M. Rahimi, N. Taheri Qazvini, B. Lin, N. Abbott, B. Roux, M. Schlossman and J. de Pablo, *J. Amer. Chem. Soc.*, 2017, **139**, 3841.
- ³⁹ C. Bishop, A. Gujral, M. F. Toney, L. Yu and M. D. Ediger, *J. Phys. Chem. Lett.*, 2019, **10**, 3536.
- ⁴⁰ B. Jerome, *Rep. Pro. Phys.*, 1991, **54**, 391.
- ⁴¹ M. F. Palermo, L. Muccioli and C. Zannoni, *Phys. Chem. Chem. Phys.*, 2015, **17**, 26149.
- ⁴² M. Lahtinen, E. Kolehmainen, J. Haarala and A. Shevchenko, *Crys. Growth Des.*, 2013, **13**, 346. See the CSD (C. R. Groom, I. J. Bruno, M. P. Lightfoot and S. C. Ward, *Acta Cryst.*, 2016, **B72**, 171.) for a complete list of known ITZ crystal structures, including polymorphs (code TEHZIP and code TEHZIP03) and solvates (code REWTUK). In all known ITZ crystal structures, the rod-like molecule is approximately 2.8 nm long, indicating the robustness of this value.
- ⁴³ L. J. Fetters, D. J. Lohse, D. Richter, T. A. Witten and A. Zirkel, *Macromolecules*, 1994, **27**, 4639.
- ⁴⁴ J. S. Chickos and W. E. Acree, *J. Phys. Chem. Ref. Data*, 2003, **32**, 519
- ⁴⁵ M. Naoki and S. Koeda, *J. Phys. Chem.*, 1989, **93**, 948.
- ⁴⁶ L. Zhu, J. Jona, K. Nagapudi and T. Wu, *Pharm. Res.*, 2010, **27**, 1558.
- ⁴⁷ D. J. Plazek and J. H. Magill, *J. Chem. Phys.*, 1966, **45**, 3038.
- ⁴⁸ I. Lyubimov, L. Antony, D. M. Walters, D. Rodney, M. D. Ediger and J. J. de Pablo, *J. Chem. Phys.*, 2015, **143**, 094502.
- ⁴⁹ S. L. Simon, J. W. Sobieski and D. J. Plazek, *Polymer*, 2001, **42**, 2555.
- ⁵⁰ A. N. Rissanou and V. Harmandaris, *Macromolecules*, 2015, **48**, 2761.
- ⁵¹ A.D. Phan, K.S. Schweizer, *J. Chem. Phys.*, 2019, **150**, 044508.
- ⁵² A.D. Phan, K.S. Schweizer, *Macromolecules*, 2019, **52**, 5192.
- ⁵³ Y. Chen, W. Zhang and L. Yu, *J. Phys. Chem. B.*, 2016, **120**, 8007.
- ⁵⁴ R. Richert and C. A. Angell, *J. Chem. Phys.* 1998, **108**, 9016.
- ⁵⁵ Q. Shi, J. Tao, J. Zhang, Y. Su, T. Cai, *Crys. Growth Des.*, 2019, **20**, 24.
- ⁵⁶ S.J. Xie, K.S. Schweizer, *Macromolecules*, 2016, **49**, 9655.
- ⁵⁷ H. K. Nienhuys and M. Bonn, *J. Phys. Chem. B.*, **2009**, **113**, 7564.
- ⁵⁸ M. S. Beasley, C. Bishop, B. J. Kasting and M. D. Ediger, *J. Phys. Chem. Lett.* 2019, **10**, 4069.
- ⁵⁹ E. Leon-Gutierrez, A. Sepúlveda, G. Garcia, M. T. Clavaguera-Mora and J. Rodríguez-Viejo, *Phys. Chem. Chem. Phys.* 2016, **18**, 8244.
- ⁶⁰ M. D. Ediger, *J. Chem. Phys.* 2017, **147**, 210901.



Vertical orientation of rod-like molecules at glass/vapor interface allows deep penetration into the bulk, slowing surface diffusion.